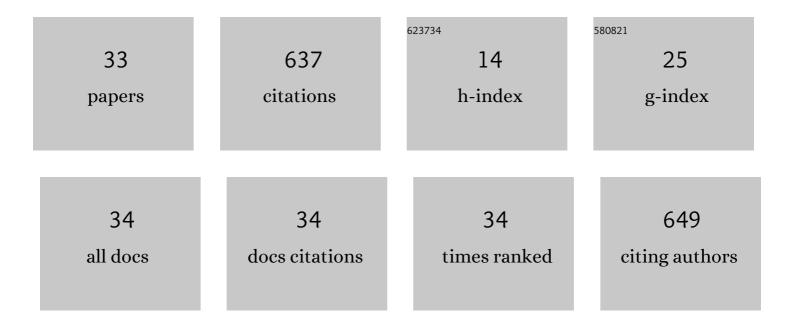
## Noriyoshi Tsujino

List of Publications by Year in descending order

Source: https://exaly.com/author-pdf/2032201/publications.pdf Version: 2024-02-01



#	Article	IF	CITATIONS
1	Deformation of Post‧pinel Under the Lower Mantle Conditions. Journal of Geophysical Research: Solid Earth, 2022, 127, .	3.4	2
2	Viscosity of bridgmanite determined by in situ stress and strain measurements in uniaxial deformation experiments. Science Advances, 2022, 8, eabm1821.	10.3	11
3	Seismic Anisotropy in the Lower Mantle Transition Zone Induced by Lattice Preferred Orientation of Akimotoite. Geophysical Research Letters, 2022, 49, .	4.0	1
4	Lattice preferred orientation of stishovite deformed at high pressure and high temperature. Physics of the Earth and Planetary Interiors, 2020, 306, 106546.	1.9	4
5	Pressure dependence of Si diffusion in Î <sup>3</sup> -Fe. American Mineralogist, 2020, 105, 319-324.	1.9	2
6	Studies of Deep Earth Rheology Based on High-Pressure Deformation Experiments Using D111-Type Apparatus. Review of High Pressure Science and Technology/Koatsuryoku No Kagaku To Gijutsu, 2020, 30, 78-84.	0.0	4
7	High-pressure generation in the Kawai-type multianvil apparatus equipped with tungsten-carbide anvils and sintered-diamond anvils, and X-ray observation on CaSnO3 and (Mg,Fe)SiO3. Comptes Rendus - Geoscience, 2019, 351, 253-259.	1.2	23
8	Phase transition of wadsleyite-ringwoodite in the Mg2SiO4-Fe2SiO4 system. American Mineralogist, 2019, 104, 588-594.	1.9	10
9	Sharp 660-km discontinuity controlled by extremely narrow binary post-spinel transition. Nature Geoscience, 2019, 12, 869-872.	12.9	31
10	Single-crystal elasticity of (Al,Fe)-bearing bridgmanite and seismic shear wave radial anisotropy at the topmost lower mantle. Earth and Planetary Science Letters, 2019, 518, 116-126.	4.4	14
11	Complete agreement of the post-spinel transition with the 660-km seismic discontinuity. Scientific Reports, 2018, 8, 6358.	3.3	27
12	Rheological Study of Bridgmanite at the Lower Mantle. Review of High Pressure Science and Technology/Koatsuryoku No Kagaku To Gijutsu, 2018, 28, 139-148.	0.0	1
13	Grain growth of $\hat{I}\mu$ -iron: Implications to grain size and its evolution in the Earth's inner core. Earth and Planetary Science Letters, 2017, 459, 238-243.	4.4	11
14	Synthesis of boron-doped diamond and its application as a heating material in a multi-anvil high-pressure apparatus. Review of Scientific Instruments, 2017, 88, 093904.	1.3	23
15	Pressure generation to 65â€GPa in a Kawai-type multi-anvil apparatus with tungsten carbide anvils. High Pressure Research, 2017, 37, 507-515.	1.2	25
16	A shallow origin of so-called ultrahigh-pressure chromitites, based on single-crystal X-ray structure analysis of the high-pressure Mg <sub>2</sub> Cr <sub>2</sub> O <sub>5</sub> phase, with modified ludwigite-type structure. American Mineralogist, 2017, 102, 2113-2118.	1.9	9
17	Effect of cation substitution on bridgmanite elasticity: A key to interpret seismic anomalies in the lower mantle. Scientific Reports, 2016, 6, 33337.	3.3	15
18	Generation of pressures over 40 GPa using Kawai-type multi-anvil press with tungsten carbide anvils. Review of Scientific Instruments, 2016, 87, 024501.	1.3	64

Noriyoshi Tsujino

#	Article	IF	CITATIONS
19	Mantle dynamics inferred from the crystallographic preferred orientation of bridgmanite. Nature, 2016, 539, 81-84.	27.8	55
20	Elastic wave velocity anomalies of anorthite in a subducting plate: In situ experiments. American Mineralogist, 2015, 100, 1856-1865.	1.9	4
21	Semiconductor diamond heater in the Kawai multianvil apparatus: an innovation to generate the lower mantle geotherm. High Pressure Research, 2014, 34, 392-403.	1.2	9
22	Effects of Al content on water partitioning between orthopyroxene and olivine: Implications for lithosphere–asthenosphere boundary. Earth and Planetary Science Letters, 2014, 400, 284-291.	4.4	24
23	High-pressure phase transitions in FeCr2O4 and structure analysis of new post-spinel FeCr2O4 and Fe2Cr2O5 phases with meteoritical and petrological implications. American Mineralogist, 2014, 99, 1788-1797.	1.9	54
24	Over 1 Mbar generation in the Kawai-type multianvil apparatus and its application to compression of (Mg0.92Fe0.08)SiO3 perovskite and stishovite. Physics of the Earth and Planetary Interiors, 2014, 228, 262-267.	1.9	55
25	Determination of Hydrogen Atoms Position in Enstatite by IR Spectra. Journal of Computer Chemistry Japan, 2014, 13, 169-170.	0.1	1
26	Equation of state of Î <sup>3</sup> -Fe: Reference density for planetary cores. Earth and Planetary Science Letters, 2013, 375, 244-253.	4.4	60
27	P-V-T relations of Â-Ca3(PO4)2 tuite determined by in situ X-ray diffraction in a large-volume high-pressure apparatus. American Mineralogist, 2013, 98, 1811-1816.	1.9	12
28	<i>Pâ€Vâ€T</i> equation of state for <i>ε</i> â€iron up to 80 GPa and 1900 K using the Kawaiâ€type high pressi apparatus equipped with sintered diamond anvils. Geophysical Research Letters, 2012, 39, .	ure 4.0	35
29	Isothermal compression of face-centered cubic iron. American Mineralogist, 2012, 97, 1417-1420.	1.9	25
30	Effect of pressure on grainâ€growth kinetics of ferropericlase to lower mantle conditions. Geophysical Research Letters, 2010, 37, .	4.0	4
31	Stress relaxation experiments of olivine under conditions of subducted slab in Earth's deep upper mantle. Physics of the Earth and Planetary Interiors, 2010, 183, 164-174.	1.9	8
32	Stress measurement under high pressure using Kawai-type multi-anvil apparatus combined with synchrotron radiation. Journal of Synchrotron Radiation, 2009, 16, 757-761.	2.4	7
33	Grain-growth kinetics of ferropericlase at high-pressure. Physics of the Earth and Planetary Interiors, 2009, 174, 145-152.	1.9	7